

# 3D Gaussian Splatting against Moving Objects for High-Fidelity Street Scene Reconstruction

Peizhen Zheng<sup>1,†</sup>   Longfei Wei<sup>1,2,†</sup>   Dongjing Jiang<sup>2</sup>   Jianfei Zhang<sup>2,1,\*</sup>

<sup>1</sup>ThinkX Canada   <sup>2</sup>MedicineX

<sup>†</sup>Equal Contribution

<sup>\*</sup>Corresponding: zhang@thinkx.ca

## Abstract

The accurate reconstruction of dynamic street scenes is critical for applications in autonomous driving, augmented reality, and virtual reality. Traditional methods relying on dense point clouds and triangular meshes struggle with moving objects, occlusions, and real-time processing constraints, limiting their effectiveness in complex urban environments. While multi-view stereo and neural radiance fields have advanced 3D reconstruction, they face challenges in computational efficiency and handling scene dynamics. This paper proposes a novel 3D Gaussian point distribution method for dynamic street scene reconstruction. Our approach introduces an adaptive transparency mechanism that eliminates moving objects while preserving high-fidelity static scene details. Additionally, iterative refinement of Gaussian point distribution enhances geometric accuracy and texture representation. We integrate directional encoding with spatial position optimization to optimize storage and rendering efficiency, reducing redundancy while maintaining scene integrity. Experimental results demonstrate that our method achieves high reconstruction quality, improved rendering performance, and adaptability in large-scale dynamic environments. These contributions establish a robust framework for real-time, high-precision 3D reconstruction, advancing the practicality of dynamic scene modeling across multiple applications. The source code for this work is available to the public at <https://github.com/thinkxca/3dgs>

## 1 Introduction

The rapid advancement of autonomous driving, augmented reality (AR), and virtual reality (VR) technologies has heightened the need for precise 3D scene reconstruction. Accurately capturing and reconstructing real-world environments, especially in complex urban settings, is essential for enhancing navigation safety, interactive experiences, and scene understanding (Schwall et al., 2020; Zhou et al., 2024). High-precision 3D street scene reconstruction plays a crucial role in autonomous driving by improving perception and decision-making in dynamic environments. Advancements

in deep learning, big data processing, and sensor technologies have significantly enhanced these capabilities, enabling better detection of buildings, roads, trees, vehicles, and pedestrians.

Traditional 3D street scene reconstruction methods primarily rely on dense point clouds or triangular meshes (Bulatov et al., 2011). These methods extract features from images or light detection and ranging (LiDAR) data captured from multiple viewpoints to generate dense 3D point clouds. While these methods can achieve high reconstruction accuracy in static environments, e.g., effectively modeling buildings, roads, and trees, they face significant challenges in dynamic scenes. Specifically, they struggle with moving objects and scene changes, often leading to inaccurate reconstructions (Bârsan et al., 2018). One major limitation of dense point cloud methods is their assumption that the scene remains static. In dynamic environments (with continuous traffic movement and changing weather conditions), these methods fail to differentiate between static backgrounds and moving objects, leading to errors where vehicles, pedestrians, or other moving elements are mistakenly incorporated into the reconstructed model. This results in unrealistic representations, distorting the overall scene and reducing credibility. Similarly, while triangular mesh methods can produce high-quality surface models, they often require complex algorithms for separating moving objects and updating the scene, making real-time processing impractical. These limitations highlight the need for more advanced approaches that enhance accuracy, efficiency, and scalability for dynamic street scene reconstruction. Addressing these challenges is a key focus of this research.

In recent years, multi-view stereo (MVS) technology (Goesele et al., 2007) has played a crucial role in 3D reconstruction by estimating scene depth from images taken from multiple viewpoints, allowing for the generation of dense 3D point clouds. Traditional MVS methods rely on image registration and geometric optimization to enhance reconstruction accuracy and completeness. However, as scene complexity and dynamism increase, MVS struggles with challenges such as rapid motion and occlusions, limiting its effectiveness in dynamic environments. Deep learning has thus been incorporated. For example, the deep multi-view stereo (DeepMVS) (Huang et al., 2018) leverages deep neural networks to learn depth information from images, improving robustness against occlusions and lighting variations that hinder traditional MVS. However, these MVS-based methods still face persistent challenges, including inconsistencies across viewpoints, difficulties in separating moving objects, and high computational costs. These issues are particularly pronounced in complex and highly dynamic street scene environments, necessitating further improvements. As research progresses, neural radiance fields (NeRF) (Müller et al., 2022) have emerged as a promising alternative for multi-view scene modeling. NeRF excels at photorealistic rendering but relies on high-density sampling and complex neural network inference, making real-time processing computationally expensive. Its ability to capture fine geometric details and distinguish moving objects in street scenes remains limited (Yang et al., 2024b). Traditional point cloud-based representations, such as explicit meshes and voxelization, have improved rendering efficiency, but they often depend on sparse point cloud initialization, reducing their adaptability in dynamic and complex scenes (Bansal and Zollhoefer, 2023; Li et al., 2021). To overcome these challenges, 3D Gaussian Splatting (3DGS) represents scenes via Gaussian distributions and therefore achieves a balance between rendering efficiency and geometric detail preservation (Zhou et al., 2024). Nevertheless, 3DGS still cannot address challenges in separating moving objects, optimizing storage requirements, and

ensuring multi-view consistency. These challenges highlight the need for further development to enhance the applicability of 3DGS in real-world dynamic environments.

In this paper, we propose a novel 3D Gaussian splitting against moving objects (GaussianMove) for high-fidelity dynamic street scene reconstruction. Our approach effectively removes moving objects by enhancing the spatial representation and encoding mechanism of Gaussian points while optimizing transparency settings in dynamic regions. Experimental results demonstrate that our method achieves high reconstruction quality and rendering efficiency in dynamic street environments. This work includes three key innovations:

- An adaptive transparency mechanism leverages multi-view consistency constraints and Gaussian distribution properties to perform mask matching and transparency optimization for moving object regions. This effectively eliminates the influence of moving objects while preserving the high-precision modeling of static backgrounds.
- By iteratively refining the distribution and transparency of Gaussian points, our framework ensures the precise removal of moving objects while progressively enhancing geometric detail and texture representation in static regions. This approach maintains an optimal balance between rendering efficiency and reconstruction fidelity.
- The approach of integrating directional encoding with spatial position optimization can minimize redundant representations and storage overhead of Gaussian points. This approach significantly reduces storage costs while maintaining high rendering efficiency and detail integrity in large-scale dynamic environments.

Our method effectively addresses the challenges of dynamic street scene reconstruction by improving accuracy, efficiency, and adaptability, making it a promising solution for real-world applications.

The rest of this paper is organized as follows. [Section 2](#) reviews related work on traditional and modern 3D reconstruction methods, including multi-view stereo (MVS), neural radiance fields (NeRF), and recent advancements in Gaussian-based scene representations. [Section 3](#) details the proposed dynamic street scene reconstruction method, introducing the adaptive transparency optimization mechanism, the progressive dynamic scene rendering framework, and the novel Gaussian point encoding and storage strategy. [Section 4](#) presents experimental evaluations, including dataset descriptions, implementation details, performance comparisons, and qualitative and quantitative results. Finally, [Section 5](#) concludes the paper by summarizing key findings and emphasizing the broader impact of our work in dynamic 3D scene reconstruction.

## 2 Related Work

This work focuses on street scene reconstruction and moving object elimination, we thus review existing methods in these domains, emphasizing their effectiveness in handling moving elements such as pedestrians and vehicles. In particular, we analyze techniques aimed to accurately eliminate moving objects while preserving the details of static backgrounds. Many of these approaches optimize transparency handling in moving object regions by integrating multi-view consistency, semantic

segmentation, and temporal sequence analysis, significantly enhancing the quality of dynamic scene modeling (Luiten et al., 2023). We also explore distributed modeling techniques based on Gaussian point distributions and highlight their advantages in reducing storage requirements, improving rendering efficiency, and mitigating uncertainties in dynamic scene reconstruction. Furthermore, we discuss the importance of progressive dynamic scene separation frameworks in achieving a balance between rendering efficiency and detail preservation (Deng et al., 2023).

## 2.1 Multi-view Stereo

Multi-View Stereo (MVS) is a technique used to reconstruct dense 3D geometric structures of a scene from multiple images with known camera poses. By leveraging these images, MVS generates highly detailed 3D representations that enable rendering from novel viewpoints. This technique plays a crucial role in various fields, including virtual reality (VR), augmented reality (AR), 3D reconstruction, robotic navigation, photogrammetry, and the digitization of cultural heritage.

Traditional MVS methods rely on explicit pixel matching, using hand-crafted image features, such as the scale-invariant feature transform (SIFT) (Lowe, 2004) and the speeded-up robust features (SURF) (Bay et al., 2006), to establish correspondences between multiple views. These methods optimize geometric and photometric consistency to produce high-quality 3D models (e.g., (Furukawa and Ponce, 2009)). However, these methods struggle in complex scenes with occlusions, sparse textures, and insufficient image redundancy, often resulting in outlier points due to matching errors (Long et al., 2022). To address these challenges, (Campbell et al., 2008) proposed an MVS approach based on multi-hypothesis depth maps. By introducing spatial consistency constraints, this method extracts accurate depths while allowing the algorithm to return an unknown state for uncertain regions, thereby avoiding unreliable depth values. By incorporating these strategies into a discrete Markov random field (MRF) optimization framework, the approach achieves high-accuracy depth maps with minimal outliers. Similarly, (Furukawa and Ponce, 2009) introduced the patch-based MVS (PMVS) method, which adopts a match-expand-filter framework. By leveraging local photometric consistency and global visibility constraints, PMVS significantly improves the quality of dense 3D reconstructions. Starting with sparse key points to generate initial patch seeds, PMVS progressively expands to cover the entire scene surface and filters erroneous matches, demonstrating exceptional robustness and adaptability.

Modern deep-learning-based MVS methods leverage neural networks to automatically extract image features and implicitly learn correspondences across multiple views in an end-to-end framework. These approaches can directly regress dense depth maps or voxel representations, significantly improving robustness in challenging scenarios with complex lighting, occlusions, and sparse textures. (Yao et al., 2018) introduced MVSNet, an end-to-end deep learning architecture designed for depth map inference from multi-view images. The network first extracts deep visual features, constructs a 3D cost volume on the reference camera frustum using differentiable homography transformations, and applies 3D convolutions for regularization and depth regression. The final depth map is further refined using the reference image. MVSNet is flexible in handling arbitrary N-view inputs by aggregating multiple features into a single cost representation based on variance-based cost metrics. Instead of relying on depth maps as intermediate representations, (Murez et al.,

2020) proposed a method to directly regress the truncated signed distance function (TSDF) from a set of RGB images with known poses. Traditional 3D reconstruction pipelines estimate depth maps before inferring complete 3D models, but (Murez et al., 2020) hypothesized that directly learning 3D representations would be more efficient. Their approach utilizes 2D convolutional neural networks (CNNs) to extract image features independently, which are then back-projected into a voxel volume using camera intrinsics and extrinsics. A 3D CNN subsequently refines the accumulated features to predict TSDF values, enabling dense and accurate 3D reconstruction with integrated semantic segmentation at minimal computational overhead. (Ding et al., 2022) introduced TransMVSNet, the first MVS method to incorporate transformers for feature matching. By framing MVS as a feature-matching problem, they developed the feature matching transformer (FMT), which employs intra-attention and inter-attention mechanisms to aggregate long-range contextual information both within and across images. To enhance adaptation to FMT, they introduced an adaptive receptive field (ARF) module, ensuring smooth feature transitions. Additionally, feature pathways connect different network stages, propagating transformed features and gradients. Pairwise feature correlation measures similarity, while an ambiguity-reducing focal loss enhances supervision. These innovations enable TransMVSNet to achieve improved accuracy and robustness in challenging MVS tasks.

## 2.2 Neural Radiance Field

Neural Radiance Fields (NeRF) (Mildenhall et al., 2021) is a revolutionary deep learning-based 3D scene representation method. NeRF models a scene as a learnable continuous density field (Tewari et al., 2022b), combining color information from view directions to generate high-quality novel view synthesis through volumetric rendering, without explicitly modeling the scene’s 3D geometry or lighting. Its core technique leverages ray marching to integrate volumetric information within a continuous field, enabling the synthesis of realistic novel view images. NeRF demonstrates strong performance, particularly in scenes with complex lighting and occlusions.

The success of NeRF has sparked widespread research in computer vision and graphics. Some studies focus on improving point sampling strategies during the volumetric rendering process. For instance, (Zhang et al., 2021) and (Xu et al., 2022) optimized sampling processes to capture details more efficiently during volumetric rendering, significantly enhancing the quality of generated images. These methods allocate more computational resources to critical regions of ray-volume interactions through intelligent distributed sampling, improving the modeling of intricate details. On the other hand, (Tewari et al., 2022a) introduced a regularization technique that imposes geometric consistency constraints, making the learned scene representation more aligned with real 3D geometry while enhancing the realism and interpretability of rendered results.

Despite its remarkable achievements in novel view synthesis, NeRF’s primary limitation lies in its high computational cost. NeRF relies on a multi-layer perceptron (MLP) as its core model (Zhu et al., 2024), encoding and computing the scene representation for each point. This process necessitates querying multiple points along each ray and processing them through the MLP, resulting in substantial computational overhead. This becomes particularly burdensome when rendering high-resolution scenes or generating a large number of novel view images, posing a significant challenge

to its practical application. To address these challenges, researchers have explored various optimization strategies. One direction involves improving scene representations to localize computations. For example, methods employing hierarchical voxel grids, hash encoding, or neural sparse fields (Müller et al., 2022) partition the global scene into smaller regions, reducing the computational burden on the MLP. These approaches have achieved orders-of-magnitude speedups by optimizing the rendering process within localized areas. Another direction involves hybrid representations, combining NeRF with explicit geometric representations such as point clouds or triangular meshes to further reduce computational demands. Research on real-time rendering is also ongoing (Deng et al., 2022). Some approaches utilize efficient hardware accelerations, such as GPUs or TPUs, and advanced ray tracing algorithms to optimize rendering speeds. However, due to the inherent complexities of ray marching and high-dimensional scene representations in volumetric rendering, real-time NeRF rendering remains a significant challenge. Future research must strike a balance between maintaining rendering quality and reducing computational costs while exploring deep learning methods that integrate hardware optimizations to achieve more efficient and practical 3D scene representations.

### 2.3 3D Gaussian Splatting

3D Gaussian Splatting (3DGS) (Kerbl et al., 2023) is an advanced scene representation technique that constructs compact, high-quality 3D models through sparse point cloud initialization, adaptive density control, and attribute optimization. These attributes include position, transparency, and anisotropic variance, enabling accurate scene reconstruction even under challenging conditions such as complex lighting, varying viewpoints, and moving objects. By optimizing each point’s parameters (Tang et al., 2023), 3DGS effectively enhances detail preservation in dynamic scenes. A key advantage of 3DGS is its efficient GPU-based renderer, which supports both forward and backward propagation, enabling real-time rendering at 1080p resolution with frame rates exceeding 30 FPS. This capability opens new possibilities for interactive and real-time 3D scene visualization. The initialization process of 3DGS heavily depends on point clouds generated by structure from motion (SfM), leveraging rich geometric information to create an accurate scene representation. However, this reliance introduces limitations, particularly in textureless or repetitive-texture environments where point cloud sparsity can degrade reconstruction quality. Additionally, interference from moving objects may introduce artifacts, necessitating adaptive rendering adjustments to mitigate these effects. Despite these challenges, 3DGS offers significant advantages over traditional MVS methods. Unlike MVS, which requires additional depth estimation steps, 3DGS directly reconstructs scenes without the need for explicit multi-view stereo data. This streamlined approach improves training efficiency and enhances reconstruction quality, making 3DGS a promising solution for efficient and realistic dynamic scene representation.

To enhance rendering performance for large-scale 3D reconstruction, GaussianPro (Cheng et al., 2024) introduces a novel approach that progressively propagates geometric information to optimize point cloud densification, demonstrating notable effectiveness in low-texture regions. This method incorporates planar loss constraints to refine the position, orientation, and size of Gaussian points, significantly mitigating the influence of moving objects and enhancing the detailed repre-

sensation of dynamic scenes. Additionally, GaussianPro optimizes both storage and computation, reducing data redundancy and computational overhead while improving rendering efficiency. However, its reliance on high-quality initial point clouds and multi-view image data presents challenges, particularly in terms of storage demands and computational efficiency for highly dynamic scenes or large-scale reconstructions. Building on this foundation, 4D Gaussian Splatting (4DGS) (Yang et al., 2024a) extends the 3DGS framework by incorporating the temporal dimension, enabling continuous modeling of dynamic scenes. By sharing Gaussian representations across time steps and integrating physical regularization, 4DGS achieves high-fidelity rendering and long-term tracking of moving objects. This approach captures temporal changes more accurately, allowing for improved modeling of motion sequences and non-rigid deformations. Compared to traditional 3DGS methods, 4DGS relies more heavily on depth information to describe continuous scene evolution, demonstrating superior performance in handling complex dynamic environments. However, the inclusion of the time dimension increases computational complexity and data acquisition requirements, posing challenges for efficient real-time dynamic scene modeling. Despite these challenges, 4DGS offers significant advantages in large-scale, highly dynamic motion scenarios, accurately capturing object trajectories, deformations, and environmental changes. Its potential applications span fields requiring long-term tracking and high-precision dynamic modeling, such as robotics, autonomous driving, and immersive virtual environments.

### 3 Proposed Method

Our method employs a structured pipeline, illustrated in [Figure 1](#), to process videos of dynamic scenes. Through four key steps, it reconstructs a high-quality static 3D scene while efficiently removing moving objects.

1. **Video Preprocessing and Segmentation:** We use the open-source software FFmpeg<sup>1</sup> to decompose the video into sequential frames. The semantic-segment-anything (SSA) model (Chen et al., 2023) is used to extract moving object masks. We manually annotate their regions using LabelMe<sup>2</sup> for precise segmentation of moving objects.
2. **Sparse Reconstruction and Gaussian Representation:** The segmented frames and masks serve as input to a structure from motion (SfM) pipeline (Snavely et al., 2006), which reconstructs a sparse point cloud of the static scene. Each point in the sparse point cloud is converted into a 3D Gaussian distribution containing position, color, and a covariance matrix, optimizing the data format for rasterization. A neural-network-inspired training process further refines the 3D Gaussian parameters (e.g., position, color, transparency), enhancing reconstruction quality.
3. **Rendering and Moving Object Elimination:** The rasterization-friendly Gaussian model translates the 3D scene into 2D images by simulating light propagation and scattering. The moving object mask is expanded into three channels to align pixel-wise with the rendered image. The transparency of moving object regions is set to zero, replacing masked areas with static back-

---

<sup>1</sup><https://www.ffmpeg.org>

<sup>2</sup><https://labelme.io>

ground colors. An iterative refinement process ensures the effective removal of moving objects while preserving background details.

4. **Optimization for Efficiency and Quality:** A region-based processing strategy divides the screen into static and dynamic regions and therefore minimizes redundant computation. 3D filtering operations reduce high-frequency artifacts introduced during scaling. Block-wise rendering enhances computational efficiency by focusing processing only on relevant pixel regions.

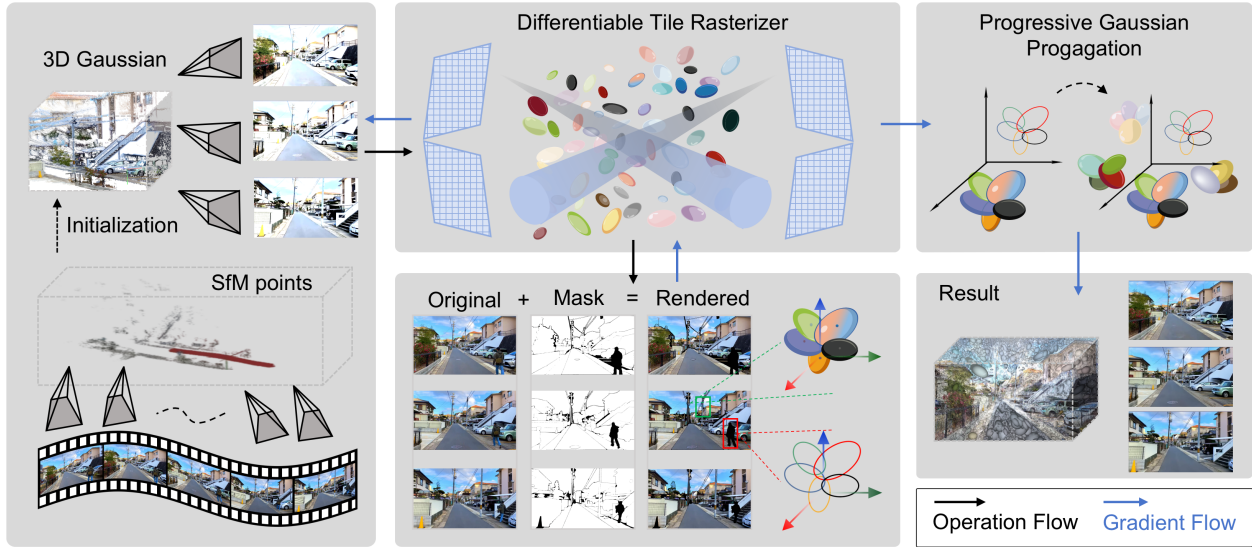


Figure 1: The generation of 3D Gaussian distributions from an SfM sparse point cloud and their subsequent projection rendering. The black arrows represent the Operation Flow, while the blue arrows indicate the Gradient Flow. By initializing sparse SfM point clouds to generate 3D Gaussian distributions, our method effectively combines the flexibility of Gaussian distribution models with the demands of dynamic scene modeling, significantly enhancing the representation of scene geometric details and dynamic regions.

### 3.1 3D Gaussian Splatting

The initialization of 3D Gaussian splatting relies on 3D point clouds, which, in dynamic environments, depend on two key technologies: structure from motion (SfM) (Snavely et al., 2006) and multi-view stereo (MVS) (Goesele et al., 2007).

- SfM extracts keyframes from an image sequence, estimates camera poses, and reconstructs sparse point clouds through feature detection, matching, and triangulation. To mitigate interference from moving objects (e.g., pedestrians, vehicles), semantic segmentation or motion detection techniques are required.
- MVS refines depth maps using multi-view images to reconstruct high-precision dense point clouds. In dynamic scenes, semantic masking or trajectory analysis of moving objects helps prevent artifacts and inaccuracies in reconstruction.

A 3D Gaussian (or 3-dimensional Gaussian distribution) is a multivariate normal distribution representing an ellipsoid in space, capable of capturing translations and rotations. This distribution is characterized by a mean vector and a covariance matrix, which define its shape, orientation, and the spread of points around the mean. In Gaussian splatting, this 3D Gaussian distribution is rasterized, projecting the 3D object (e.g., an ellipsoid) onto a 2D plane, where the result is a splat—a graphical representation in 2D. The splat, formed by the projection of the 3D Gaussian, allows for efficient 3D-to-2D transformation in rendering applications, with each Gaussian distribution contributing to the pixel values based on its color, transparency, and spatial characteristics (Yifan et al., 2019), as follows:

$$G(\mathbf{x}) = \exp\left(-\frac{1}{2}(\mathbf{x} - \boldsymbol{\mu})^\top \boldsymbol{\Sigma}^{-1}(\mathbf{x} - \boldsymbol{\mu})\right). \quad (1)$$

In this context, the Gaussian’s mean  $\boldsymbol{\mu} \in \mathbb{R}^{3 \times 1}$  and covariance  $\boldsymbol{\Sigma} \in \mathbb{R}^{3 \times 3}$  control the scaling and rotation of the ellipsoid in 3D space. The mean vector  $\boldsymbol{\mu}$  determines the center of the Gaussian, while the covariance matrix  $\boldsymbol{\Sigma}$  defines the spread and orientation of the distribution, transforming the Gaussian from a spherical to an ellipsoidal shape, initialized as

$$\boldsymbol{\Sigma} = \mathbf{R}\mathbf{S}\mathbf{S}^\top \mathbf{R}^\top, \quad (2)$$

where the rotation matrix  $\mathbf{R} \in \mathbb{R}^{3 \times 3}$  is orthogonal, and the scale matrix  $\mathbf{S} \in \mathbb{R}^{3 \times 3}$  is diagonal. To render an image from a given viewpoint, the color of pixel  $\mathbf{p}$  can be computed by blending the contributions of the ordered Gaussians  $\{G_i\}_{i=1}^N$  based on their projected colors and transparencies, as follows:

$$\mathbf{c}(\mathbf{p}) = \sum_{i \in N} \mathbf{c}_i \alpha_i \prod_{j=1}^{i-1} (1 - \alpha_j). \quad (3)$$

The opacity  $\alpha_i$  of the  $i$ -th Gaussian  $G_i$  typically ranges from 0 (fully transparent) to 1 (fully opaque). It is based on the Gaussian’s density and distance to the camera. The  $\mathbf{c}_i$  is the color contribution of  $G_i$ , typically determined by the Gaussian’s color parameter (often obtained from the texture or surface color associated with the 3D point).

## 3.2 Mask Computation and Object Elimination

The presence of moving objects in the 3D Gaussian splatting process can degrade the quality of static background reconstruction. To address this issue, we leverage a mask computation method that accurately identifies and removes moving object regions, adjusting their transparency to either replace them with the background color or make them fully transparent.

- We first employ the segment anything model (SAM) to generate a binary mask  $M(p)$ , where  $M(p) = 1$  indicates the pixel  $p$  corresponds to the background region, and  $M(p) = 0$  marks the moving object region.
- To eliminate residual edges and small gaps in the moving object regions, we apply morphological dilation on the binary mask. The dilation operation expands the boundary of moving object regions, ensuring a more complete coverage of moving objects. This is done using the following formula:

$$M(p) = \max_{p' \in \mathcal{N}(p)} M(p'),$$

where  $\mathcal{N}(p)$  is the neighborhood window of pixel  $p$ , and a typical structuring element for dilation is a  $3 \times 3$  or  $5 \times 5$  window.

- **Mask-Based Color and Transparency Control in Rendering.** The mask  $M(p)$  is used during the 3DGS rendering stage to control pixel color and transparency, ensuring that moving objects do not interfere with the reconstruction of the static background. For each pixel  $p$ , the rendered color is adjusted based on the mask value: If  $M(p) = 1$ , we retain the original rendered color; If  $M(p) = 0$ , we replace the rendered color with the background color  $C = C_{\text{bg}}(p)$ . This is computed as:

$$C(p) = C_{\text{render}}(p) \cdot \overline{M}(p) + C_{\text{bg}}(p) \cdot M(p),$$

where  $C_{\text{render}}(p)$  is the original rendered color, and  $\overline{M}(p)$  represents the Boolean negation of  $M(p)$ .

- **Transparency Adjustment for Moving Objects.** In addition to color adjustment, we set the transparency of moving object regions to fully transparent to further ensure they do not impact the final rendered image. This is achieved by:

$$\alpha(p) = \alpha_{\text{render}}(p) \cdot \overline{M}(p),$$

where  $\alpha_{\text{render}}(p)$  is the original rendering opacity of the rendered image. For moving object regions (where  $M(p) = 0$ ), the transparency is set to zero, effectively making these regions invisible in the rendered result.

### 3.3 Progressive Gaussian Propagation

The progressive Gaussian propagation strategy is a highly effective method for optimizing the geometry of 3D scene modeling. Its primary goal is to iteratively propagate accurate geometric information from well-modeled regions to areas that are under-modeled or poorly represented, creating new Gaussian distributions in the process. This strategy employs patch matching techniques (Bleyer et al., 2011) to transfer depth and normal information from neighboring pixels to the current pixel, generating propagated depth and propagated normals. By progressively refining these areas, the method enhances geometric accuracy and improves the global consistency of the 3D scene.

- The method starts by constructing the local geometric information for each pixel using the rendered depth and normal maps. This step provides an initial understanding of the scene’s geometry.
- Patch matching techniques are then applied to define the local plane for each pixel. The depth and normal information are converted into local plane parameters in 3D space. Geometric transformations and color consistency evaluations are used to progressively propagate depth and normal information to under-modeled regions. This ensures that the most accurate geometric candidates are selected, improving the overall geometric consistency of the scene.
- Following propagation, geometric filtering and screening are employed to enhance the reliability of the results. This involves performing multi-view geometric consistency checks to filter out potential errors or noise introduced during the propagation step. The depth and normal maps are refined, ensuring a more accurate and consistent representation of the scene’s geometry.

- For regions where the difference between the filtered results and the original depth map exceeds a predefined threshold, it is assumed that the existing Gaussian models cannot accurately represent the geometric structure of these areas. In these regions, pixels are projected back into 3D space, and new Gaussian models are initialized to supplement the existing models. This step improves the coverage and accuracy of the model.
- The newly generated Gaussians are integrated with the existing models, and further optimization is applied to enhance the overall quality of the scene’s geometry. This continuous refinement ensures that the final scene representation is both detailed and globally consistent.

### 3.3.1 Plane Definition

The propagation combines the pixel’s depth information with its normal direction, accurately describing the position of the plane where the pixel resides. This forms the foundation for subsequent geometric propagation and optimization. Meanwhile, the use of homogeneous coordinates and transformations with the camera intrinsic matrix  $\mathbf{K}$  ensures the method’s adaptability and generalization across different camera models. For pixel  $p$  and its coordinate  $\mathbf{p}$ , the corresponding local 3D plane is parameterized as  $(d, \mathbf{n})$ , where  $\mathbf{n}$  is the rendered normal of the pixel, and  $d$  is the distance between the camera coordinate and the local plane. The calculation is given by

$$d = \delta \mathbf{n}^\top \mathbf{K}^{-1} \tilde{\mathbf{p}}. \quad (4)$$

Here,  $\tilde{\mathbf{p}}$  is the homogeneous coordinates of the pixel  $p$ ,  $\delta$  is the pixel’s rendered depth, and  $\mathbf{K}$  is the camera intrinsic matrix. After defining the 3D local plane, an efficient and symmetric neighborhood selection strategy is adopted to facilitate effective information propagation. This strategy involves selecting the neighborhood of each pixel as the foundation for propagation, allowing for the acquisition of a candidate set of planes.

### 3.3.2 SSIM-based Patch Matching

During the patch matching process, for each pixel  $p$  and its corresponding image patch in the candidate plane, we evaluate image consistency between pixel coordinate  $\mathbf{p}$  and the coordinate  $\mathbf{p}'$  of its  $Q$  neighboring pixels  $\{p_{b_q} : q = 1, 2, \dots, Q\}$  using a similarity metric. To transform the candidate plane  $(d_{b_q}, \mathbf{n}_{b_q})$ , we warp  $\mathbf{p}$  to  $\mathbf{p}'$  in the neighboring frame using a homography matrix  $H$ :

$$\begin{aligned} \tilde{\mathbf{p}}' &\approx \mathbf{H} \tilde{\mathbf{p}} \\ \mathbf{H} &= \mathbf{K} \left( \mathbf{W}_{\text{rel}} - \frac{\mathbf{t}_{\text{rel}} \mathbf{n}_{b_q}^\top}{d_{b_q}} \right) \mathbf{K}^{-1} \end{aligned}$$

Here,  $[\mathbf{W}_{\text{rel}}, \mathbf{t}_{\text{rel}}]$  denotes the relative transformation from the reference view to the neighboring view.

For each candidate plane’s corresponding image patch, the Structural Similarity Index (SSIM) is used to assess image consistency between pixel coordinates  $\mathbf{p}$  and  $\mathbf{p}'$ . SSIM is computed between the reference image and the adjacent image on the candidate planes, and the plane with the highest

SSIM value is selected as the optimal plane for the current pixel. This optimal plane’s depth and normal are then chosen to ensure accurate geometric propagation. Unlike other metrics, SSIM is robust to lighting changes and noise, making it ideal for stable matching in complex scenes. Additionally, SSIM aligns with human perception of image distortions, especially in texture-rich regions, where it better captures structural details. The SSIM formula is given by:

$$\text{SSIM}(I_i, I_j) = \frac{(2\boldsymbol{\mu}_i\boldsymbol{\mu}_j + a_1)(2\boldsymbol{\Sigma}_{ij} + a_2)}{(\boldsymbol{\mu}_i^2 + \boldsymbol{\mu}_j^2 + a_1)(\boldsymbol{\Sigma}_i^2 + \boldsymbol{\Sigma}_j^2 + a_2)}, \quad (5)$$

where  $\boldsymbol{\mu}_i$  and  $\boldsymbol{\mu}_j$  are the mean luminance of images  $I_i$  and  $I_j$ ,  $\boldsymbol{\Sigma}_i$  and  $\boldsymbol{\Sigma}_j$  are their luminance variances, and  $\boldsymbol{\Sigma}_{ij}$  is their luminance covariance. These values capture the structural similarity, with  $a_1$  and  $a_2$  stabilizing the formula when the denominator approaches zero.

### 3.4 Learning Objective

To optimize the quality of the generated results, this paper introduces a set of loss functions that enhance the accuracy of geometric modeling and image reconstruction through multidimensional constraints. The total learning loss  $\mathcal{L}$  includes the image reconstruction losses  $L_1$  and  $L_2$  in 3DGS, along with a combined constraint loss  $\ell_*$ , expressed as:

$$\mathcal{L} = (1 - \lambda)L_1 + \lambda L_2 + \lambda_* \ell_*.$$

The loss  $L_1$  measures the pixel-wise difference between the generated and original images in the visible region, defined as

$$L_1 = \frac{1}{|\mathcal{V}|} \sum_{I \in \mathcal{V}} \|I - \phi(I)\|,$$

where  $I$  represents the pixel value at coordinate  $p$  in the original image, and  $\phi(I)$  denotes the pixel value for the reconstructed image. The set  $\mathcal{V}$  represents all valid pixels in the visible region. The  $L_2$  loss, also referred to as the DSSIM loss, is defined as the inverse metric of the Structural Similarity Index (SSIM), i.e.,

$$L_2 = \frac{1}{|\mathcal{V}|} \sum_{I \in \mathcal{V}} (1 - \text{SSIM}(I, \phi(I))). \quad (6)$$

This loss improves the perceptual similarity between the generated and ground truth images.

For  $\ell_*$ , it can be one of  $\ell_{\text{flatten}}$ ,  $\ell_{\text{sparse}}$ ,  $\ell_{\text{normal}}$ , or their combinations. The loss  $\ell_{\text{flatten}}$  minimizes the discrepancy between the predicted 3D Gaussian splats and their 2D projections, improving projection consistency. Given the scale  $S_i$  associated with  $G_i$  and the predefined upper limit of the scale  $S_{\text{max}}$ , the flattening loss constrains the scale variation to ensure smooth geometric distribution by a comparison between  $S$  and  $S_{\text{max}}$  as follows:

$$\ell_{\text{flatten}} = \frac{1}{N} \sum_{i=1}^N |\min(S_i, S_{\text{max}})|. \quad (7)$$

The loss  $\ell_{\text{sparse}}$  encourages sparsity in 3D Gaussian representation, reducing the number of splats needed to represent the scene. This loss function decreases computational complexity and prevents overfitting by applying an information entropy constraint, defined as

$$\ell_{\text{sparse}} = -\frac{1}{N} \sum_{i=1}^N \left( \alpha_i \log \alpha_i + (1 - \alpha_i) \log(1 - \alpha_i) \right). \quad (8)$$

The loss  $\ell_{\text{normal}}$  optimizes the geometric consistency between the generated normals and the original normals, as detailed in (Long et al., 2020).

## 4 Experiments

We present the data, evaluation metrics, and comparative experimental results and analysis.

### 4.1 Data

We utilize two real-world videos in our experiments.

- Nogoya video captured a modern community in Nagoya City, Aichi Prefecture, Japan, showcases a large-scale, boundaryless outdoor environment<sup>3</sup>. We sampled 60 frames from 13:26 to 13:38.
- Québec video recorded in the Royal Square of Québec City, Québec, Canada, also presents a large-scale, boundaryless outdoor scene<sup>4</sup>. A total of 98 frames were sampled from 1:13 to 1:33.

Both videos contain dynamic and static objects, with moving objects primarily consisting of pedestrians and moving vehicles, while static objects include vehicles, houses, and roads. Pedestrians exhibit walking motion, while the houses and vehicles offer rich visual references. The videos present challenges such as dynamic scene complexity, occlusion (objects being obstructed), and lighting variations. Data preprocessing involves resolution adjustment, manual annotation, and data augmentation (e.g., rotation, scaling, and brightness adjustment) to improve the model’s robustness in complex environments.

### 4.2 Setup

This research is built upon the open-source 3DGS project code implementation. The model was trained for 30,000 iterations specifically for dynamic scenes, utilizing the geometric structures and hyperparameter settings provided by 3DGS, with the absolute relative error threshold ( $\sigma$ ) set to 0.8. The implementation incorporates the cloning and splitting Gaussian densification strategy from 3DGS, as well as the 3-stage progressive propagation strategy. To prevent interference from Gaussian ellipsoids generated in the mask region, the design omits mask processing, ensuring a static effect for dynamic scenes and enhancing the model’s adaptability in complex dynamic environments. The entire implementation is based on the PyTorch-GPU open-source framework, developed in a Python environment, and experiments were conducted on an NVIDIA RTX 4070 GPU.

<sup>3</sup><https://youtu.be/qv7L0rXFrXk>

<sup>4</sup><https://www.bilibili.com/video/BV1ij28YqEe8>

### 4.3 Evaluation Metrics

In the experiment, we evaluate the model’s performance using PSNR (Peak Signal-to-Noise Ratio) (Yuanji et al., 2003), SSIM (Structural Similarity Index) (Wang et al., 2004), and LPIPS (Learned Perceptual Image Patch Similarity) (Zhang et al., 2018). PSNR is a widely-used metric that measures the similarity between processed images (such as compressed, denoised, or restored) and the original image. Expressed in decibels (dB), higher PSNR values indicate less distortion, meaning the processed image is closer to the original.

SSIM, in contrast, aligns better with human visual perception, taking into account structure, luminance, and contrast sensitivity. The SSIM value ranges from -1 to 1, where 1 indicates perfect similarity, 0 indicates no structural similarity, and negative values indicate highly dissimilar structures. A higher SSIM value indicates that the processed image is closer to the original.

Additionally, LPIPS is used as a perceptual evaluation metric. Unlike traditional pixel-level metrics (such as MSE or PSNR), LPIPS assesses perceptual similarity using deep features extracted through a pre-trained neural network, offering a more accurate reflection of visual quality. A lower LPIPS value signifies less perceptual distortion, meaning the processed image visually resembles the original more closely.

## 4.4 Results

### 4.4.1 Comparisons

Our method significantly outperforms other techniques across all evaluation metrics on the Nagoya video dataset. The presence of moving objects in the street scene poses a challenge to accurate 3D scene reconstruction. To mitigate this, we use Structure from Motion (SfM) to generate an initial point cloud, effectively removing noise caused by moving objects. However, in conventional 3DGS methods, the iterative comparison of processed images with real images during rasterization still allows moving objects in the real images to influence the generation of point clouds and ellipsoid sets, resulting in unavoidable artifacts. In contrast, our method employs moving object masking, effectively preventing noise generation. The background is then used to fill in and restore the 3D street scene, ensuring the construction of a high-quality, efficient static scene.

Table 1: Comparison of models’ performance

| Model                             | PSNR         | SSIM        | LPIPS       | FPS        |
|-----------------------------------|--------------|-------------|-------------|------------|
| Mip-Nerf360 (Barron et al., 2022) | 22.52        | 0.86        | 0.13        | 0.08       |
| Zip-NeRF (Barron et al., 2023)    | 23.62        | 0.85        | 0.14        | 0.32       |
| 3DGS (Kerbl et al., 2023)         | 21.50        | 0.78        | 0.18        | 121        |
| GaussianPro (Cheng et al., 2024)  | 22.45        | 0.88        | 0.13        | 108        |
| VEGS (Hwang et al., 2024)         | 23.32        | 0.81        | 0.14        | 108        |
| GaussianMove (Ours)               | <b>23.35</b> | <b>0.89</b> | <b>0.13</b> | <b>108</b> |

**Table 1** presents the performance of various models in terms of image quality metrics, including PSNR, SSIM, and LPIPS. Our method (Ours) consistently outperforms all others, achieving a PSNR of 23.35, an SSIM of 0.89, and the lowest LPIPS of 0.13, highlighting its superior image reconstruction quality and structural similarity. In comparison, Mip-Nerf360 and Zip-Nerf excel in PSNR and SSIM but fall slightly behind in LPIPS. VEGS shows PSNR and SSIM values close to ours but delivers lower overall quality. 3DGS demonstrates weaker performance across all three metrics, while GaussianPro performs similarly to our method in SSIM but lags behind in PSNR and LPIPS. In conclusion, our method offers a significant improvement in image quality, with high PSNR, superior SSIM, and low LPIPS.

**Figure 2** and **Figure 3** show original images from the Nagoya and Québec videos, respectively. In Nagoya, the pedestrian in **Figure 2** is the only moving object to be removed. The images generated by 3DGS, GaussianPro, VEGS, and our method revealed that 3DGS, GaussianPro, and VEGS still retain subtle artifacts from moving objects. In contrast, our method effectively eliminates these artifacts, achieving a high-quality static street scene reconstruction. In Québec, the moving objects in **Figure 3** include both vehicles and pedestrians. The three competing methods seem capable of eliminating only the pedestrians, while our method successfully removes both pedestrians and vehicles entirely.



**Figure 2:** Comparison of elimination of moving objects by our method and competitors in the reconstruction of the video for Nagoya scene.



**Figure 3:** Comparison of elimination of moving objects by our method and competitors in reconstructing the video for Québec scene.

**Figure 4** and **Figure 5** display five original frames (top) from both videos and the reconstructed frames (bottom) produced by our method. Our method consistently removes moving objects while generating clearer images than the originals. Notably, for the static vehicle in **Figure 5(a)**, our method accurately recognizes it as static and preserves while performing high-quality reconstruction.



Figure 4: Comparison between original images (top) and reconstructed images after removing moving objects by our method in the video for Nagoya city.



Figure 5: Comparison between original images (top) and reconstructed images after removing moving objects in the video for Québec city. The vehicle highlighted by the green box in column (a) is a static object and thus retained, while all other vehicles and pedestrians marked by the red box in columns (b)-(e) are moving objects and eliminated by our method.

#### 4.4.2 Ablation Study

In this ablation study, we aim to optimize the parameter configuration for the 3D Gaussian Splatting technique by evaluating the effects of different loss functions. Specifically, we examine three key loss functions:  $\ell_{\text{flatten}}$ ,  $\ell_{\text{sparse}}$ , and  $\ell_{\text{normal}}$ , both individually and in combination. Each loss function targets a specific aspect of the 3D scene representation, contributing to enhanced reconstruction accuracy and rendering efficiency.

The analysis of the impact of different loss functions on 3D Gaussian Splatting (3DGS) reveals that each loss function individually affects performance metrics such as PSNR, SSIM, and LPIPS. This indicates that each loss function focuses on distinct aspects during optimization, influencing the final reconstruction accuracy and rendering efficiency. When  $\ell_{\text{flatten}}$  and  $\ell_{\text{sparse}}$  are used individually, their performance is relatively lower, particularly in terms of PSNR and SSIM. However, significant improvements are observed when these loss functions are combined. For example, combining  $\ell_{\text{flatten}}$  and  $\ell_{\text{sparse}}$  results in a PSNR of 22.22 and an SSIM of 0.84, indicating that this combination effectively enhances reconstruction quality. The joint use of  $\ell_{\text{flatten}}$ ,  $\ell_{\text{sparse}}$ , and  $\ell_{\text{normal}}$  achieves the highest

Table 2: Performance of our approach with various combinations of loss

| $\ell_{\text{flatten}}$ | $\ell_{\text{sparse}}$ | $\ell_{\text{normal}}$ | PSNR         | SSIM        | LPIPS       |
|-------------------------|------------------------|------------------------|--------------|-------------|-------------|
| $\times$                | $\times$               | $\times$               | 21.20        | 0.82        | 0.15        |
| $\checkmark$            | $\times$               | $\times$               | 21.20        | 0.85        | 0.14        |
| $\times$                | $\checkmark$           | $\times$               | 22.10        | 0.84        | 0.14        |
| $\times$                | $\times$               | $\checkmark$           | 21.82        | 0.83        | 0.15        |
| $\checkmark$            | $\checkmark$           | $\times$               | 22.22        | 0.84        | 0.13        |
| $\checkmark$            | $\times$               | $\checkmark$           | 22.82        | 0.87        | 0.12        |
| $\times$                | $\checkmark$           | $\checkmark$           | 23.24        | 0.80        | 0.13        |
| $\checkmark$            | $\checkmark$           | $\checkmark$           | <b>23.31</b> | <b>0.89</b> | <b>0.13</b> |

PSNR of 23.31, an SSIM of 0.89, and minimizes LPIPS to 0.13, demonstrating the effectiveness of our loss settings.

## 5 Conclusion

This paper proposes a dynamic street scene reconstruction method based on 3D Gaussian point distribution technology. By leveraging adaptive transparency optimization for moving object regions, a progressive dynamic scene rendering framework, and a novel Gaussian point encoding and storage mechanism, the method achieves high-fidelity dynamic scene reconstruction and moving object removal.

The proposed method effectively mitigates interference from moving objects through adaptive transparency optimization, coupled with multi-view consistency constraints and the inherent properties of Gaussian distributions. This allows for precise modeling of the background and static scene elements. Simultaneously, the progressive dynamic scene rendering framework optimizes moving object removal and enhances static scene details by incrementally adjusting Gaussian point distribution and transparency settings. The novel Gaussian point encoding and storage mechanism, integrating directional encoding and spatial location optimization, significantly reduces redundancy and storage requirements, ensuring efficient rendering performance and geometric integrity in large-scale dynamic scenes.

Experimental results demonstrate that the proposed method outperforms traditional approaches in terms of dynamic street scene reconstruction accuracy, rendering efficiency, and moving object separation capability. It provides an efficient and accurate solution for dynamic scene modeling and rendering in applications such as autonomous driving, high-precision map generation, virtual and augmented reality, and smart city development. This method not only addresses the limitations of traditional dynamic scene processing techniques but also offers valuable insights and technical support for efficient modeling of complex dynamic scenes in the future.

## References

- Aayush Bansal and Michael Zollhoefer. Neural pixel composition for 3D-4D view synthesis from multi-views. In *IEEE/CVF Conference on Computer Vision and Pattern Recognition (CVPR)*, pages 290–299, 2023.
- Jonathan T. Barron, Ben Mildenhall, Dor Verbin, Pratul P. Srinivasan, and Peter Hedman. Mip-NeRF 360: Unbounded anti-aliased neural radiance fields. In *IEEE/CVF Conference on Computer Vision and Pattern Recognition (CVPR)*, pages 5460–5469, 2022.
- Jonathan T. Barron, Ben Mildenhall, Dor Verbin, Pratul P. Srinivasan, and Peter Hedman. Zip-NeRF: Anti-aliased grid-based neural radiance fields. In *IEEE/CVF International Conference on Computer Vision (ICCV)*, pages 19640–19648, 2023.
- Ioan Andrei Bârsan, Peidong Liu, Marc Pollefeys, and Andreas Geiger. Robust dense mapping for large-scale dynamic environments. In *IEEE International Conference on Robotics and Automation (ICRA)*, pages 7510–7517, 2018.
- Herbert Bay, Tinne Tuytelaars, and Luc Van Gool. SURF: Speeded up robust features. In *European Conference on Computer Vision (ECCV)*, pages 404–417, 2006.
- Michael Bleyer, Christoph Rhemann, and Carsten Rother. Patchmatch stereo - stereo matching with slanted support windows. In Jesse Hoey, Stephen J. McKenna, and Emanuele Trucco, editors, *British Machine Vision Conference (BMVC)*, pages 1–11, 2011.
- Dimitri Bulatov, Peter Wernerus, and Christian Heipke. Multi-view dense matching supported by triangular meshes. *ISPRS Journal of Photogrammetry and Remote Sensing (ISPRS)*, 66(6):907–918, 2011.
- Neill DF Campbell, George Vogiatzis, Carlos Hernández, and Roberto Cipolla. Using multiple hypotheses to improve depth-maps for multi-view stereo. In *European Conference on Computer Vision (ECCV)*, pages 766–779, 2008.
- Jiaqi Chen, Zeyu Yang, and Li Zhang. Semantic segment anything. <https://github.com/fudan-zvg/Semantic-Segment-Anything>, 2023.
- Kai Cheng, Xiaoxiao Long, Kaizhi Yang, Yao Yao, Wei Yin, Yuexin Ma, Wenping Wang, and Xuejin Chen. Gaussianpro: 3d gaussian splatting with progressive propagation. In *International Conference on Machine Learning (ICML)*, 2024.
- Kangle Deng, Andrew Liu, Jun-Yan Zhu, and Deva Ramanan. Depth-supervised nerf: Fewer views and faster training for free. In *IEEE/CVF Conference on Computer Vision and Pattern Recognition (CVPR)*, pages 12882–12891, 2022.
- Tianchen Deng, Siyang Liu, Xuan Wang, Yejia Liu, Danwei Wang, and Weidong Chen. Prosgnerf: Progressive dynamic neural scene graph with frequency modulated auto-encoder in urban scenes. *arXiv preprint arXiv:2312.09076*, 2023.
- Yikang Ding, Wentao Yuan, Qingtian Zhu, Haotian Zhang, Xiangyue Liu, Yuanjiang Wang, and Xiao Liu. Transmvsnet: Global context-aware multi-view stereo network with transformers. In *IEEE/CVF Conference on Computer Vision and Pattern Recognition (CVPR)*, pages 8585–8594, 2022.

- Yasutaka Furukawa and Jean Ponce. Accurate, dense, and robust multiview stereopsis. *IEEE Transactions on Pattern Analysis and Machine Intelligence (PAMI)*, 32(8):1362–1376, 2009.
- Michael Goesele, Noah Snavely, Brian Curless, Hugues Hoppe, and Steven M. Seitz. Multi-view stereo for community photo collections. In *IEEE International Conference on Computer Vision (ICCV)*, pages 1–8, 2007.
- Po-Han Huang, Kevin Matzen, Johannes Kopf, Narendra Ahuja, and Jia-Bin Huang. Deepmvs: Learning multi-view stereopsis. In *IEEE Conference on Computer Vision and Pattern Recognition (CVPR)*, pages 2821–2830, 2018.
- Sungwon Hwang, Min-Jung Kim, Taewoong Kang, Jayeon Kang, and Jaegul Choo. VEGS: View extrapolation of urban scenes in 3D gaussian splatting using learned priors. *CoRR*, abs/2407.02945, 2024.
- Bernhard Kerbl, Georgios Kopanas, Thomas Leimkühler, and George Drettakis. 3d gaussian splatting for real-time radiance field rendering. *Communications of the Association for Computing Machinery (CACM)*, 42(4):139:1–139:14, 2023.
- Zhengqi Li, Simon Niklaus, Noah Snavely, and Oliver Wang. Neural scene flow fields for space-time view synthesis of dynamic scenes. In *IEEE/CVF Conference on Computer Vision and Pattern Recognition (CVPR)*, pages 6498–6508, 2021.
- Xiaoxiao Long, Lingjie Liu, Christian Theobalt, and Wenping Wang. Occlusion-aware depth estimation with adaptive normal constraints. In *European Conference on Computer Vision (ECCV)*, pages 640–657, 2020.
- Xiaoxiao Long, Cheng Lin, Peng Wang, Taku Komura, and Wenping Wang. Sparseneus: Fast generalizable neural surface reconstruction from sparse views. In *European Conference on Computer Vision (ECCV)*, pages 210–227, 2022.
- David G Lowe. Distinctive image features from scale-invariant keypoints. *International Journal of Computer Vision (IJCV)*, 60:91–110, 2004.
- Jonathon Luiten, Georgios Kopanas, Bastian Leibe, and Deva Ramanan. Dynamic 3D gaussians: Tracking by persistent dynamic view synthesis. *arXiv preprint arXiv:2308.09713*, 2023.
- Ben Mildenhall, Pratul P Srinivasan, Matthew Tancik, Jonathan T Barron, Ravi Ramamoorthi, and Ren Ng. Nerf: Representing scenes as neural radiance fields for view synthesis. *Communications of the Association for Computing Machinery (CACM)*, 65(1):99–106, 2021.
- Thomas Müller, Alex Evans, Christoph Schied, and Alexander Keller. Instant neural graphics primitives with a multiresolution hash encoding. *Communications of the Association for Computing Machinery (CACM)*, 41(4):102:1–102:15, 2022.
- Zak Murez, Tarrence Van As, James Bartolozzi, Ayan Sinha, Vijay Badrinarayanan, and Andrew Rabinovich. Atlas: End-to-end 3D scene reconstruction from posed images. In *IEEE/CVF Conference on Computer Vision and Pattern Recognition (CVPR)*, pages 414–431, 2020.
- Matthew Schwall, Tom Daniel, Trent Victor, Francesca Favaro, and Henning Hohnhold. Waymo public road safety performance data. *arXiv preprint arXiv:2011.00038*, 2020.

- Noah Snavely, Steven M. Seitz, and Richard Szeliski. Photo tourism: Exploring photo collections in 3D. *Communications of the Association for Computing Machinery (CACM)*, 25(3):835–846, 2006.
- Jiaxiang Tang, Jiawei Ren, Hang Zhou, Ziwei Liu, and Gang Zeng. Dreamgaussian: Generative gaussian splatting for efficient 3D content creation. *arXiv preprint arXiv:2309.16653*, 2023.
- Ayush Tewari, Justus Thies, Ben Mildenhall, Pratul Srinivasan, Edgar Tretschk, Wang Yifan, Christoph Lassner, Vincent Sitzmann, Ricardo Martin-Brualla, Stephen Lombardi, et al. Advances in neural rendering. *Computer Graphics Forum*, 41(2):703–735, 2022a.
- Ayush Tewari, Justus Thies, Ben Mildenhall, Pratul P. Srinivasan, Edgar Tretschk, Yifan Wang, Christoph Lassner, Vincent Sitzmann, Ricardo Martin-Brualla, Stephen Lombardi, Tomas Simon, Christian Theobalt, Matthias Nießner, Jonathan T. Barron, Gordon Wetzstein, Michael Zollhöfer, and Vladislav Golyanik. Advances in neural rendering. *COMPUTER GRAPHICS FORUM*, 41(2):703–735, 2022b.
- Zhou Wang, Alan C. Bovik, Hamid R. Sheikh, and Eero P. Simoncelli. Image quality assessment: from error visibility to structural similarity. *IEEE Transactions on Image Processing*, 13(4):600–612, 2004.
- Qiangeng Xu, Zexiang Xu, Julien Philip, Sai Bi, Zhixin Shu, Kalyan Sunkavalli, and Ulrich Neumann. Point-NeRF: Point-based neural radiance fields. In *IEEE/CVF Conference on Computer Vision and Pattern Recognition (CVPR)*, pages 5428–5438, 2022.
- Zeyu Yang, Hongye Yang, Zijie Pan, and Li Zhang. Real-time photorealistic dynamic scene representation and rendering with 4d gaussian splatting. In *International Conference on Learning Representations (ICLR)*, 2024a.
- Ziyi Yang, Xinyu Gao, Wen Zhou, Shaohui Jiao, Yuqing Zhang, and Xiaogang Jin. Deformable 3D gaussians for high-fidelity monocular dynamic scene reconstruction. In *IEEE/CVF Conference on Computer Vision and Pattern Recognition (CVPR)*, pages 20331–20341, 2024b.
- Yao Yao, Zixin Luo, Shiwei Li, Tian Fang, and Long Quan. Mvsnet: Depth inference for unstructured multi-view stereo. In *European Conference on Computer Vision (ECCV)*, pages 767–783, 2018.
- Wang Yifan, Felice Serena, Shihao Wu, Cengiz Öztireli, and Olga Sorkine-Hornung. Differentiable surface splatting for point-based geometry processing. *ACM Transactions on Graphics: The Journal of the ACM Special Interest Group on Computer Graphics (SIGGRAPH)*, 38(6):1–14, 2019.
- Wang Yuanji, Li Jianhua, Lu Yi, Fu Yao, and Jiang Qinzong. Image quality evaluation based on image weighted separating block peak signal to noise ratio. In *International Conference on Neural Networks and Signal Processing (ICNSP)*, volume 2, pages 994–997. IEEE, 2003.
- Richard Zhang, Phillip Isola, Alexei A. Efros, Eli Shechtman, and Oliver Wang. The unreasonable effectiveness of deep features as a perceptual metric. In *IEEE Conference on Computer Vision and Pattern Recognition (CVPR)*, pages 586–595, 2018.
- Xiuming Zhang, Pratul P. Srinivasan, Boyang Deng, Paul E. Debevec, William T. Freeman, and Jonathan T. Barron. NeRFactor: Neural factorization of shape and reflectance under an unknown

illumination. *Communications of the Association for Computing Machinery (CACM)*, 40(6): 237:1–237:18, 2021.

Xiaoyu Zhou, Zhiwei Lin, Xiaojun Shan, Yongtao Wang, Deqing Sun, and Ming-Hsuan Yang. Drivinggaussian: Composite gaussian splatting for surrounding dynamic autonomous driving scenes. In *IEEE/CVF Conference on Computer Vision and Pattern Recognition (CVPR)*, pages 21634–21643, 2024.

Hanxin Zhu, Tianyu He, Xin Li, Bingchen Li, and Zhibo Chen. Is vanilla mlp in neural radiance field enough for few-shot view synthesis. In *IEEE/CVF Conference on Computer Vision and Pattern Recognition (CVPR)*, pages 20288–20298, 2024.